FakeCatcher: Detection of Synthetic Portrait Videos using Biological Signals

Umur Aybars Ciftci, İlke Demir, and Lijun Yin, *Senior Member, IEEE*

Abstract—The recent proliferation of fake portrait videos poses direct threats on society, law, and privacy [1]. Believing the fake video of a politician, distributing fake pornographic content of celebrities, fabricating impersonated fake videos as evidence in courts are just a few real world consequences of deep fakes. We present a novel approach to detect synthetic content in portrait videos, as a preventive solution for the emerging threat of *deep fakes*. In other words, we introduce a deep fake detector. We observe that detectors blindly utilizing deep learning are not effective in catching fake content, as generative models produce formidably realistic results. Our key assertion follows that biological signals hidden in portrait videos can be used as an implicit descriptor of authenticity, because they are neither spatially nor temporally preserved in fake content. To prove and exploit this assertion, we first engage several signal transformations for the pairwise separation problem, achieving 99.39% accuracy. Second, we utilize those findings to formulate a generalized classifier for fake content, by analyzing proposed signal transformations and corresponding feature sets. Third, we generate novel signal maps and employ a CNN to improve our traditional classifier for detecting synthetic content. Lastly, we release an "in the wild" dataset of fake portrait videos that we collected as a part of our evaluation process. We evaluate FakeCatcher on several datasets, resulting with 96%, 94.65%, 91.50%, and 91.07% accuracies, on Face Forensics [2], Face Forensics++ [3], CelebDF [4], and on our new Deep Fakes Dataset respectively. In addition, our approach produces a significantly superior detection rate against baselines, and does not depend on the source, generator, or properties of the fake content. We also analyze signals from various facial regions, under image distortions, with varying segment durations, from different generators, against unseen datasets, and under several dimensionality reduction techniques.

Index Terms—deep fakes, generative models, biological signals, authenticity classification, fake detection, image forensics.

1 Introduction

As we enter into the artifical intelligence (AI) era, the technological advancements in deep learning started to revolutionize our perspective on how we solve difficult problems in computer vision, robotics, and related areas. In addition, the developments in generative models (i.e., [5], [6], [7], [8]) empower machines to increase the photorealism in the generated data and mimic the world more accurately. Even though it is easy to speculate dystopian scenarios based on both analysis and synthesis approaches, the latter brought the immediate threat on information integrity by disabling our "natural detectors": we cannot simply look at an image to determine its authenticity.

Following the recent initiatives for democratization of AI, generative models become increasingly popular and accessible. The widespread use of generative adversarial networks (GAN) is positively impacting some technologies: it is very easy to create personalized avatars [9], to produce animations [10], and to complete and stylize images [11]. Unfortunately, they are also used with malicious intent. The famous deep fake Obama video warning us about deep fakes going viral [12] may be the most innocent example, but there are far more devastating real-world examples which impact the society by introducing inauthentic content such as fake celebrity porn [13], political misinformation through fake news [14], and forfeiting art using AI [15]. This lack of authenticity and increasing information obfuscation pose real threats to individuals, criminal system, and information integrity. As every technology is simultaneously built with the counter-technology to neutralize its negative effects, we believe that it is the perfect time to develop a deep fake detector to battle with deep fakes before having serious consequences.

We can regard counterfeiting money as an analogy. Actual bills are stamped with an unknown process so that fake money can not contain that special mark. We are looking for that special mark in authentic videos, which are already stamped by physics and biology of the real world, but generative models yet to replicate in image space because they "do not know" how the stamp works. As an example of such special marks, the chaotic order of the real world is found as an authenticity stamp by the study of Benes et al. [16]. As another example, Pan et al. [17] defend the same idea and propose integrating physics-based models for GANs to improve the realism of the generated samples. Biological signals (such as heart rate) have already been exploited for medical [18] and security purposes [19], therefore we wonder: *Can we depend on the biological signals as our authenticity stamps? Do generative models capture biological signals? If not, can we formulate how and why they fail to do so?*

We observe that, even though GANs learn and generate photorealistic visual and geometric signals beyond the discriminative capabilities of human eyes, biological signals hidden by nature are still not easily replicable. Biological signals are also intuitive and complimentary ingredients of facial videos – which is the domain of deep fakes. Moreover, videos, as opposed to images, contain another layer of complexity to becloud fake synthesis: the consistency in the time dimension. Together with the signals' spatial coherence, temporal consistency is the key prior to detect

- *Umur Aybars Ciftci and Lijun Yin are with the Department of Computer Science, Binghamton University, Binghamton, NY.*
- *Ilke Demir is a Senior Research Scientist at Intel Corporation, CA. E-mail: {uciftci,lijun}@binghamton.edu, idemir@purdue.edu*

Manuscript received Sept. 11, 2019; revised May 12; accepted July 4, 2020.

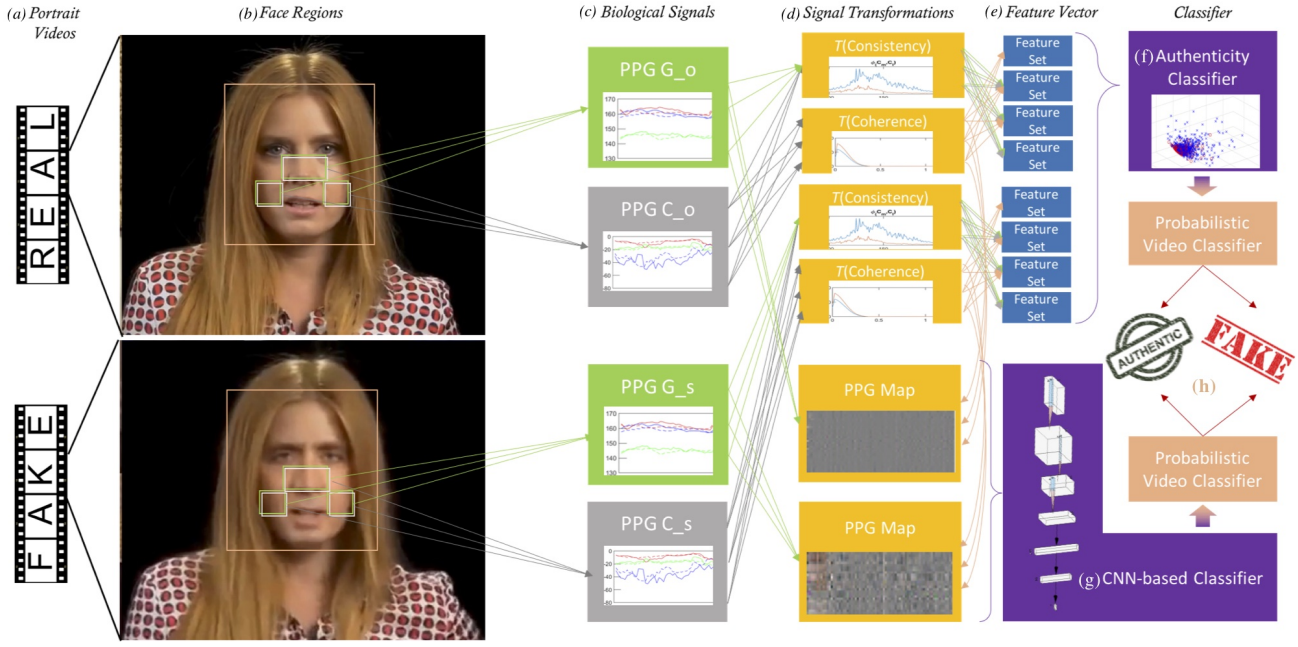

Fig. 1: **Overview.** We extract biological signals (c) from face regions (b) of authentic and fake portrait video pairs (a). We apply transformations (d) to compute spatial coherence and temporal consistency, capture signal characteristics in feature sets (e) and PPG maps, and train a probabilistic SVM (f) and a CNN (g). Then, we aggregate authenticity probabilities (h) to classify the authenticity.

authentic content. Although there are recent pure deep learning approaches to detect fake content, those are limited by the specific generative model [20], dataset [2], people [21], or hand-crafted features [22]. In contrast to all, we choose to search for some natural priors in authentic content, instead of putting some assumptions on the fake content. To complete this narrative, our approach exploits biological signals to detect fake content in portrait videos, independent of the source of creation.

Our main contributions include,

- formulations and experimental validations of signal transformations to exploit spatial coherence and temporal consistency of biological signals, for both pairwise and general authenticity classification,
- a generalized and interpretable deep fake detector that operates in-the-wild,
- a novel biological signal map construction to train neural networks for authenticity classification,
- a diverse dataset of portrait videos to create a test bed for fake content detection in the wild.

Our system processes input videos (Figure 1a) by collecting fixed-length video segments with facial parts, defining regions of interests within each face (Figure 1b), and extracting several biological signals (Figure 1c) from those regions in those temporal segments. In the first part of our paper, we scrutinize the pairwise separation problem where video pairs are given but the fake one is not known. We formulate a solution by examining the extracted biological signals, their transformations to different domains (time, frequency, time-frequency), and their correlations (Figure 1d). In the second part, we combine the revelations from the pairwise context and interpretable feature extractors in the literature (Figure 1e) to develop a generalized authenticity classifier working in a high dimensional feature space (Figure 1f). In the third part, we transform the signals into novel signal maps of fixed-duration segments to train a simple convolutional deep fake detector network (Figure 1g). We also aggregate the class probabilities of segments in a video into a binary "fake or authentic" decision (Figure 1h).

To evaluate FakeCatcher, we collected over 140 online videos, totaling up to a "Deep Fakes Dataset" of 30GB. It is important to note that, unlike existing datasets, our dataset includes "in the wild" videos, independent of the generative model, resolution, compression, content, and context. Our simple convolutional neural network (CNN) achieves 91.07% accuracy for detecting inauthentic content on our dataset, 96% accuracy on Face Forensics dataset (FF) [2], and 94.65% on Face Forensics++ (FF++) [3] dataset, outperforming all baseline architectures we compared against. We also analyzed the effects of segment durations, facial regions, face detector, image distortions, and dimensionality reduction techniques on mentioned datasets.

2 Related Work

Traditionally, image spoofing and forgery has been an important topic in forensics and security, with corresponding pixel and frequency analysis solutions to detect visual artifacts [23]. These methods, in addition to early deep generative models, were able to create some inauthentic content. However, results were easily classified as fake or real by humans, as opposed to deep fakes.

2.1 GAN Empowerment

Following GANs proposed by Goodfellow et al. [5], deep learning models have been advancing in generative tasks for inpainting [24], translation [7], and editing [25]. Inherently, all generative approaches suffer from the control over generation. In the context of GANs, this problem is mostly explored by Variational Autoencoders (VAE) [26] and Conditional GANs [27] to control the generation by putting constraints in the latent space. In addition to the improvements in controlling GANs, other approaches

improved training efficiency, accuracy, and realism of GANs by deep convolutions [6], Wasserstein distances [28], least squares [29], and progressive growing [30]. It is arguable that these developments, in addition to the availability of such models, seeded the authenticity problem.

2.2 Synthetic Faces

Since Viola-Jones [31], computer vision community treasures the domain of facial images and videos as one of the primary application areas. Therefore, numerous applications and explorations of GANs emerged for face completion [11], facial attribute manipulation [32], [33], [34], frontal view synthesis [35], facial reenactment [36], [37], [38], identity-preserving synthesis [39], and expression editing [40]. In particular, advancements in generative power, realism, and efficiency of VAEs and GANs for facial reenactment and video synthesis resulted in the emergence of the "deep fake" concept, which is replacing the face of a target person with another face in a given video, as seamless as possible. The exact approach is not published, however the deep fake generator is assumed to consist of two autoencoders trained on source and target videos: Keeping the encoder weights similar, so that general features can be embedded in the encoder and face-specific features can be integrated by the decoder. Another approach, Face2Face [37], reconstructs a target face from a video and then warps it with the blend shapes obtained by the source video in real-time. Deep Video Portraits [36] and vid2vid [8] follow this approach and employ GANs instead of blend shapes. Overall, the results are realistic, but there are still skipped frames and face misalignments due to illumination, occlusion, compression, and sudden motions.

2.3 Image Forensics

In par with the increasing number of inauthentic facial images and videos, methods for detecting such have also been proposed. Those are mostly based on finding inconsistencies in images, such as detecting distortions [41], finding compression artifacts [42], and assessing image quality [43]. However, for synthetic images in our context, the noise and distortions are harder to detect due to the non-linearity and complexity of the learning process [44].

There exist two different strategies to tackle this problem, (i) pure deep learning based approaches that act as a detector of a specific generative model [20], [45], [46], [47], [48], [49], [50], and (ii) semantic approaches that evaluate the generated faces' realism [22], [51], [52]. We summarize all of these in Table 1. The methods in the first branch investigate the color and noise distributions of specific networks [53], [54], [55] or specific people [21], or train CNNs blindly for synthetic images [20], [45], [50]. However, they are unfit to be accepted as general synthetic portrait video detection mechanisms, as they rely heavily on detecting artifacts inherent to specific models. Semantic approaches, on the other hand, utilize inconsistencies in the biological domain, such as facial attributes [51], [56], mouth movement inconsistency [52], and blink detection [22]. Our motivation follows the second stream, however we explore real signals instead of physical attributes. Thus our input is continuous, complex, and stable; making our system embrace both perspectives.

2.4 Biological Signals

The remote extraction of biological signals roots back to the medical community to explore less invasive methods for patient monitoring. Observing subtle changes of color and motion in RGB videos [65], [66] enable methods such as color based remote photoplethysmography (rPPG or iPPG) [67], [68] and head motion based ballistocardiogram (BCD) [69]. We mostly focus on photoplethysmography (PPG) as it is more robust against dynamically changing scenes and actors, while BCD can not be extracted if the actor is not still (i.e., sleeping). Several approaches proposed improvements over the quality of the extracted PPG signal and towards the robustness of the extraction process. The variations in proposed improvements include using chrominance features [70], green channel components [71], optical properties [72], kalman filters [73], and different facial areas [67], [71], [72], [74].

We believe that all of these PPG variations contain valuable information in the context of fake videos. In addition, inter-consistency of PPG signals from various locations on a face is higher in real videos than those in synthetic ones. Multiple signals also help us regularize environmental effects (illumination, occlusion, motion, etc.) for robustness. Thus, we use a combination of G channel-based PPG (or G-PPG, or G_*) [71] where the PPG signal is extracted only from the green color channel of an RGB image (which is robust against compression artifacts); and chrominance-based PPG (or C-PPG, or C_*) [70] which is robust against illumination artifacts.

Ref.	Accuracy	Dataset	Limitation
[20]	98%	Own, NA	only [57]
[20]	95%	FF [2]	only [37]
[45]	93.99 AUROC	celebA [58] & [9]	image only
[46]	97.1%	Own, NA	unpaired
[47]	99.60%	FF [2]	only [37] & image only
[47]	46.39% ERR	Own, NA	only [59] & [60], image only
[48]	92%	Own, NA	image only
[49]	0.927 AUC	Own, NA	only [59] & [60], image only
[51]	0.851 AUC	Own, NA	image only
[51]	0.866 AUC	FF [2]	image only
[52]	24.74% EER	temp. vidTimit [61]	audio only
[52]	33.86% EER	temp. AMI [62]	audio only
[52]	14.12% EER	temp. grid [63]	audio only
[22]	99%	Own, NA	only 50 videos
[50]	99%	FF [2]	only [37] & image only
[55]	97%	UADFV [56]	only [56] & image only
[55]	99.9%	DF-TIMIT [64]	only [64] & image only
[21]	0.95 AUC	Own, NA	person dependent
[56]	0.974 AUROC	UADFV [56]	only [56] & image only

TABLE 1: **Image Forensics.** Recent approaches with their reported accuracies on the corresponding datasets.

2.5 Deep Fake Collections

As the data dependency of GANs increases, their generative power increases, so detection methods' need for generated samples increases. Such datasets are also essential for the evaluation of novel methodologies, such as ours. Based on the release date and the generative methods, there are two generations of datasets which significantly differ in size and source.

The first generation includes (i) UADFV [56], which contains 49 real and 49 fake videos generated using FakeApp [75]; (ii) DF-TIMIT [64], which includes 620 deep fake videos from 32 subjects using facewap-GAN [76]; and (iii) Face Forensics [2] (FF) which has original and synthetic video pairs with the same content and actor, and another compilation of original and synthetic videos, all of which are created using the same generative model [37]. The train/validation/test subsets of FF are given as 704 (70%), 150 (15%) and 150 (15%) real/fake video pairs respectively.

The second generation aims to increase the generative model diversity while also increasing the dataset size. Face Forensics++ [3] dataset employs 1000 real youtube videos and generates the same number of synthetic videos with four generative models, namely Face2Face [37], Deepfakes [57], FaceSwap [59] and Neural Textures [77]. Google/Jigsaw dataset [78] contains 3068 synthetic videos based on 363 originals of 28 individuals using an unrevealed method. Lastly, Celeb-DF [4] dataset consists of 590 real and 5639 synthetic videos of 59 celebrities, generated by swapping faces using [57]. We point out the class imbalance for this dataset, as we will explore its side effects in some results.

For our experiments, analysis, and evaluation, we use two datasets from each generation; namely UADFV, FF, FF++, and Celeb-DF, in addition to our own Deep Fakes Dataset.

3 Biological Signal Analysis on Fake & Authentic Video Pairs

We employ six signals $S = \{G_L, G_R, G_M, C_L, C_R, C_M\}$ that are combinations of G-PPG [71] and C-PPG [70] on the left cheek, right cheek [72], and mid-region [74]. Each signal is named with channel and face region in subscript. Figure 2 demonstrates those signals extracted from a real-fake video pair, where each signal is color-coded with the facial region it is extracted from. We declare signals in Table 2 and transformations in Table 3.

Symbol	Signal
S	$\{G_L, G_R, G_M, C_L, C_R, C_M\}$
S_C	$\{C_L, C_R, C_M\}$
D	$\{\|C_L - G_L\|, \|C_R - G_R\|, \|C_M - G_M\|\}$
D_C	$\{\|C_L - C_M\|, \|C_L - C_R\|, \|C_R - C_M\|\}$

TABLE 2: **Signal Definitions.** Signals used in all analysis.

In order to understand the nature of biological signals in the context of synthetic content, we first compare signal responses in original (PPG_o) and synthetic (PPG_s) video pairs using traditional signal processing methods: log scale (L), Butterworth filter [79] (H), power spectral density (P), and combinations (Figure 4). We start by comparing signals (top) and their derivatives (bottom) and formulate that distinction (i.e., fourth column shows contrasting structure for their power spectra). Here, the preservation of spatial coherence and temporal consistency is observed in authentic videos, and an error metric that encapsulates these findings in a generalized classifier is desired. This analysis also sets ground for understanding generative systems in terms of biological replicability.

Symbol	Transformation
$A(S)$	autocorrelation
$\hat{A}(S)$	spectral autocorrelation
$\phi(S_x, S_y)$	cross correlation
$P(S)$	power spectral density
$A_p(S_C)$	pairwise cross spectral densities
$L(S)$	log scale
$\mathrm{X}(S)$	discrete cosine transform
$W(S)$	Wavelet transform
$Y(S)$	Lyapunov function [80]
$G(S)$	Gabor-Wigner transform [81]

TABLE 3: **Transformation Definitions.** Transformation functions used throughout the analysis of signals specified in Table 2.

3.1 Statistical Features

We set our first task as the pairwise separation problem: Given pairs of fake and authentic videos without their labels, can we take advantage of biological signals for labeling these videos? We use 150 pairs in the provided test subset of Face Forensics [2] as a base, splitting each video into ω-length temporal segments (the value for ω is extensively analyzed in Section 6.1). Our analysis starts by comparing simple statistical properties such as mean(μ), standard deviation(σ), and min-max ranges of G_M and C_M from original and synthetic video pairs. We observed the values of simple statistical properties between fake and real videos and selected the optimal threshold as the valley in the histogram of these values (Figure 3, first row). By simply thresholding, we observe an initial accuracy of 65% for this pairwise separation task. Then, influenced by the signal behavior (Figure 4), we make another histogram of these metrics on all absolute values of differences between consecutive frames for each segment (i.e., $\mu(|G_M(t_n) - G_M(t_{n+1})|)$), achieving 75.69% accuracy again by finding a cut in the histogram (Figure 3, second row). Although histograms of our implicit formulation per temporal segment is informative, a generalized detector can benefit from multiple signals, multiple facial areas, multiple frames in a more complex space. Instead of reducing all of this information to a single number, we conclude that exploring the feature space of these signals can yield a more comprehensive descriptor for authenticity.

3.2 Power Spectra

In addition to analyzing signals in time domain, we also investigate their behavior in frequency domain. Thresholding their power spectrum density ($P(S)$) in linear and log scales results in an

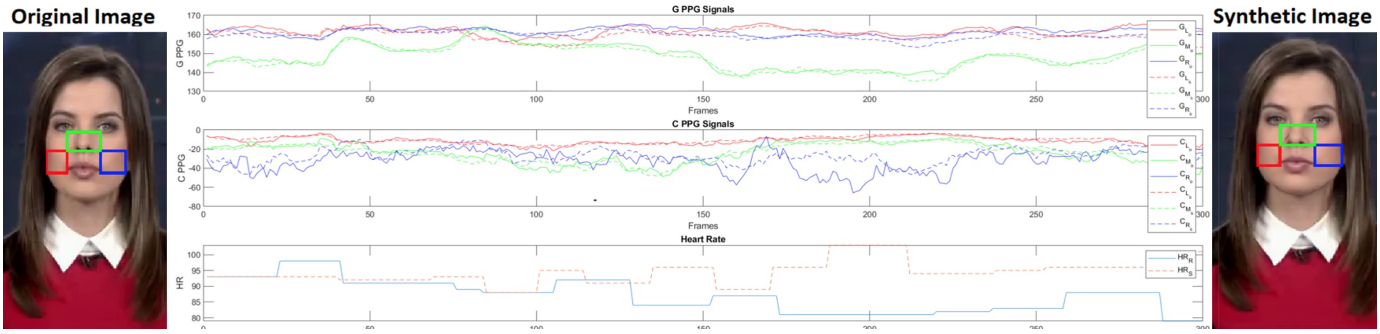

Fig. 2: **Biological Signals.** Green (G_* - top) and chrom-PPG (C_* - middle) from left ($*_L$ - red), middle ($*_M$ - green), and right ($*_R$ - blue) regions. Heart rates (HR_* - bottom), and sample frames of original (left, $*_{*_O}$ - solid) and synthetic (right, $*_{*_S}$ - dashed) videos.

accuracy of 79.33% (similar to Figure 3, third row) using the following formula:

$$\mu_{P(G_{L_o})} + \sigma_{P(G_{L_o})} - (\mu_{P(G_{L_s})} + \sigma_{P(G_{L_s})}) \quad (1)$$

where the definition of P can be found in Table 3 and G_L can be found in Table 2, and subscripts denote G_{L_o} for original and G_{L_s} for synthetic. We also analyze discrete cosine transforms (DCT) (X) of the log of these signals. Including DC and first three AC components, we obtain 77.41% accuracy (Section 6.6.4). We further improve the accuracy to 91.33% by using only zero-frequency (DC value) of X.

3.3 Spatio-temporal Analysis

Combining previous two sections, we also run some analysis for the coherence of biological signals within each signal segment. For robustness against illumination, we alternate between C_L and C_M (Table 2), and compute cross-correlation of their power spectral density as $\phi(P(C_M), P(C_L))$. Comparing their maximum

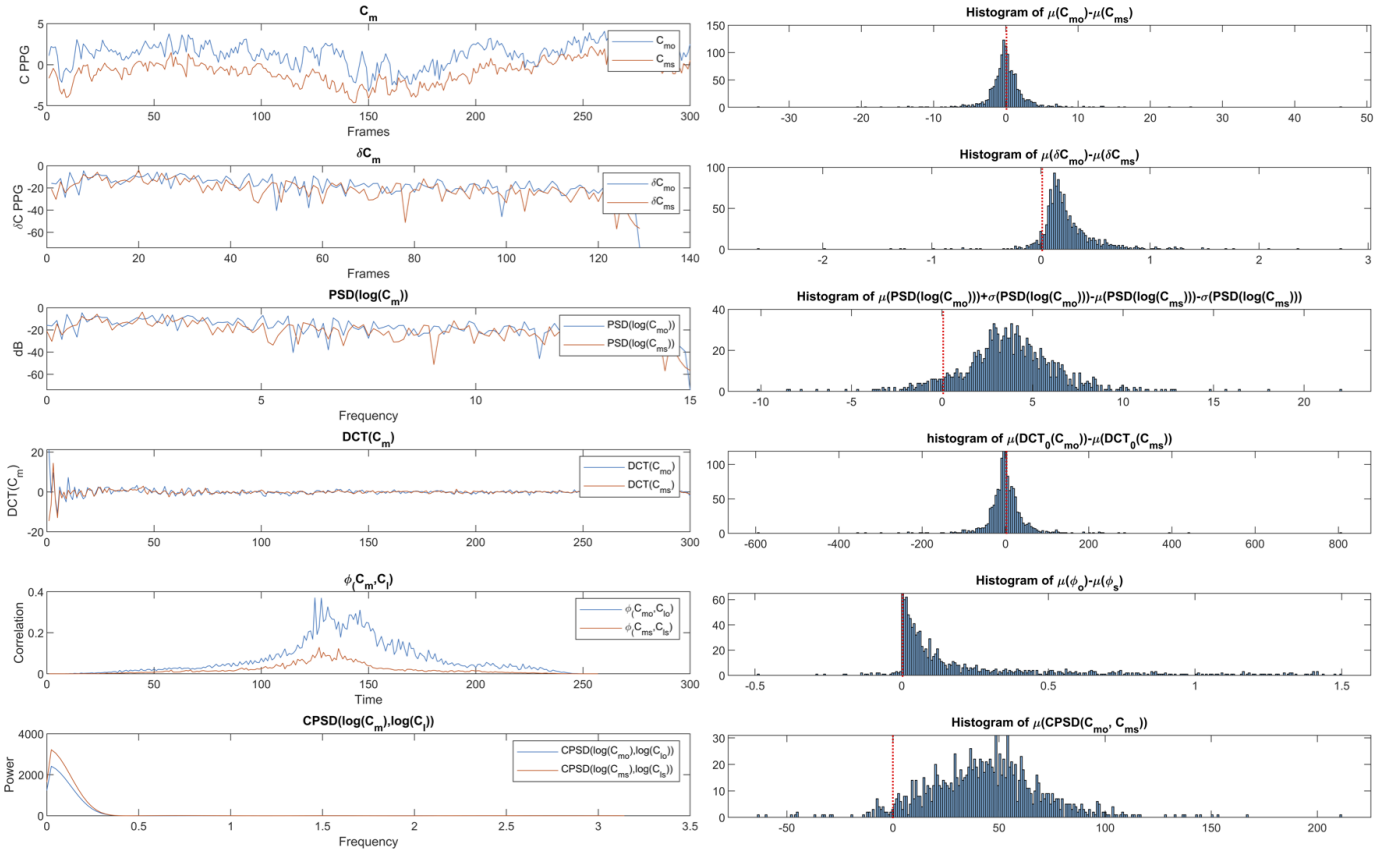

Fig. 3: **Pairwise Analysis.** Example original and synthetic signal pair C_{M_o} and C_{M_s}, their derivatives δC_M, power spectral densities $P(L(C_M))$, discrete cosine transforms $\mathrm{X}(C_M)$, cross correlation $\phi(C_M, C_L))$, and cross power spectral density $A_p(S_C)$ (left). Histograms of mean differences of these values for all pairs in the dataset (right).

Feature	Explanation	Reference
F_1	mean and maximum of cross spectral density	Sec. 3.3
F_2	RMS of differences, std., mean of absolute differences, ratio of negative differences, zero crossing rate, avg. prominence of peaks, std. prominence of peaks, avg. peak width, std. peak width, max./min. derivative, mean derivative, mean spectral centroid	[82]
F_3	nb of narrow pulses in spectral autocorrelation, nb of spectral lines in spectral autocorrelation, average energy of narrow pulses, max. spectral autocorrelation	[83]
F_4	std., std. of mean values of 1 sec windows, RMS of 1 sec differences, mean std. of differences std. of differences, mean of autocorrelation, Shannon entropy	[84]
F_5	first n Wavelet coefficients $W(S)$	[80], [85]
F_6	largest n Lyapunov exponents $Y(S)$	[80]
F_7	max. of spectral power density of normalized centered instantaneous amplitude, std. of abs. value of the centered non-linear component of instantaneous phase, std. of centered non-linear component of direct instantaneous phase, std. of abs. value of normalized centered instantaneous amplitude, kurtosis of the normalized instantaneous amplitude	[86]
F_8	log scale power of delta (1-4HZ), theta (4-8HZ), and alpha (8-13HZ) bands	[87]
F_9	mean amplitude of high frequency signals, slope of PSD curves between high and low frequencies, variance of inter-peak distances	[88]

TABLE 4: **Feature Sets.** Feature sets (left) from all experiments are explained (middle) and documented by a reference (right).

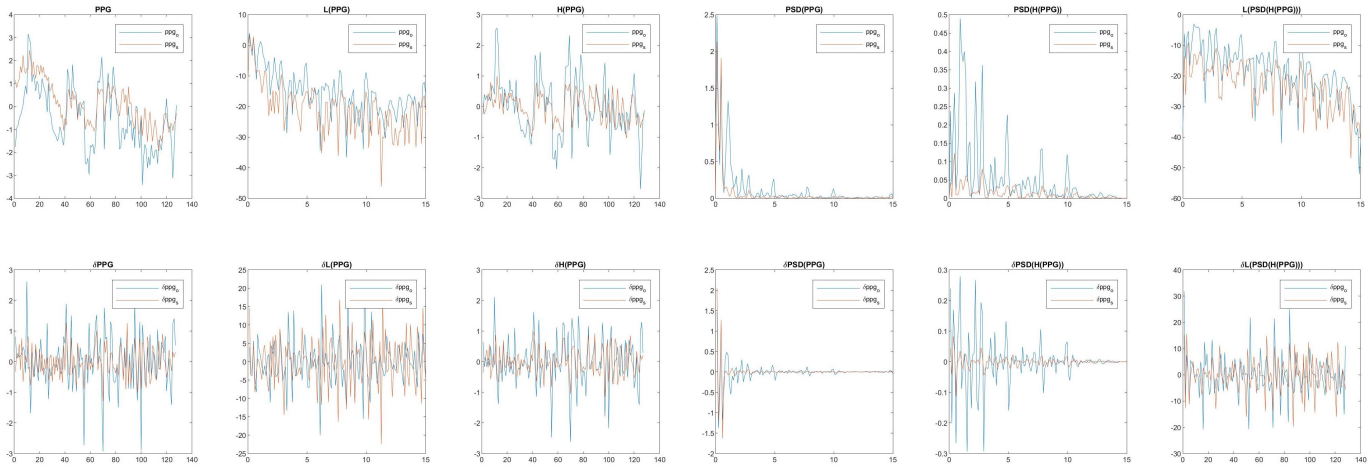

Fig. 4: **Raw Signals.** Characteristics of biological signals (top), same analysis on derivative of signals (bottom), from original (blue) and synthetic (orange) video pairs.

values gives 94.57% and mean values gives 97.28% accuracy for pairwise separation. We improve this result by first computing power spectral densities in log scale $\phi(L(P(C_M)), L(P(C_L)))$ (98.79%), and even further by computing cross power spectral densities $\mu(A_p(L(S_{C_o})) - A_p(L(S_{C_s})))$ (99.39%). Last row in Figure 3 demonstrates that difference, where 99.39% of the pairs have an authentic video with more spatio-temporally coherent biological signals. This final formulation results in an accuracy of 95.06% on the entire Face Forensic dataset (train, test, and validation sets), and 83.55% on our Deep Fakes Dataset.

4 Generalized Content Classifier

We hypothesize that our metric to separate pairs of original and synthetic videos with an accuracy of 99.39% is a promising candidate to formulate the inconsistency into a generalized binary classifier. In the pairwise setting, comparison of aggregate spatio-temporal features are representative enough. However, as these signals are continuous and noisy, there is no universal hard limit to robustly classify such content. To build a generalized classifier, we experiment with several signal transformations in time and frequency domains (as defined in Table 3) to explore the artifacts of synthetic content towards characteristic feature sets (Table 4).

4.1 Feature Sets

We explored several features to be extracted from the signals declared in Table 3. Due to the fact that rPPG is mostly evaluated by the accuracy in heart rate, we consult other features used in image authenticity [44], classification of Electroencephalography (EEG) signals [85], [87], statistical analysis [82], [83], [86], and emotion recognition [80], [87]. These feature sets are enumerated in Table 4 together with the reference papers for biological signal classification. We exhaustively document all possible feature extractors in the literature for robustness and we refer the reader to specific papers for the formulation and explanation of the features.

4.2 Authenticity Classification

Following our motivation to understand biological signals in the context of fake content, we covet interpretable features with no assumption on the fake content. This is the key that leads us to employ support vector mahine (SVM) with a radial basis function (RBF) kernel [89] for this binary classification task, instead of a DNN. We conduct many experiments by training an SVM using feature vectors extracted from the training set, and then report the accuracy of that SVM on the test set. All of these experiments are denoted with $F_*(T(S))$ where F_* is the feature extractor from Table 4 applied to (transformed) signal $T(S)$ from Table 3. Both signal transformation and feature extraction can be applied to all elements of the inner set.

For exploration, we combine all subsets of Face Forensics (FF) dataset [2] and randomly split the combined set to train (1540 samples, 60%) and test sets (1054 samples, 40%). We create feature vectors with maximum and mean (F_1) of cross power spectral densities of S_C ($A_p(S_C)$) for all videos in the train set, as it was the feature with the highest accuracy from Section 3.3. Unlike pairwise results, SVM accuracy with $f = F_1(A_p(S_C))$ is low (68.93%) but this sets a baseline for next steps. Next, we classify by $f = \mu_{P(S)}$ (six features per sample) achieving 68.88% accuracy, and by $f = \mu_{A_p(D_C)} \cup \mu_{A(S)}$ (9 features) achieving 69.63% accuracy on the entire FF dataset. Table 5 lists 7 of 70 experiments done using a combination of features. These chronologically higher results indicate the driving points of our experimentation, each of these led us to either pursue a feature set, or leave it out completely. The other 63 experiments, both on FF dataset and our Deep Fakes Dataset, are listed in Section 5.2.3.

f	$\|f\|$	$\tilde{f}$
$F_3(\hat{A}(S))$	4×6	67.55%
$F_6(L(S))$	600	69.04%
$F_4(log(S))$	60	69.07%
$F_2(S)$	13×6	69.26%
$F_5(P(W(S)))$	390	69.63%
$F_4(S) \cup$ $F_3(log(S)) \cup$ $\mu_{A_p(D_C)}$	$6 \times 6 +$ $4 \times 6 +$ 3	71.34%
$F_4(log(S) \cup A_p(D_C)) \cup$ $\cup F_1(log(D_C)) \cup$ $F_3(log(S) \cup A_p(D_C))$	$6 \times 9 +$ $6 +$ 4×9	72.01%

TABLE 5: **Experiments.** $< F_n$ from Table 4> (<transformation from Table 3> (<signal from Table 2>)) (left), size of feature vector (middle), and highest achieved segment classification accuracy (right) of some experiments.

Based on our experiments, we conclude that "authenticity" (i) is observed both in time and frequency domains, (ii) is highly sensitive to small changes in motion, illumination, and compression if a single signal source is used, and (iii) can be discovered from coherence and consistency of multiple biological signals. We infer conclusion (i) from high classification results when $A(.)$, $\hat{A}(.)$, and F_4 in time domain is used in conjunction with $P(.)$, $A_p(.)$, and F_3 in frequency domain; (ii) from low true negative numbers when only S is used instead of D_C or D, or only using F_5 or F_6, and (iii) from high accuracies when D_C, $\phi(.)$, $A_p(.)$, and F_1 is used to correlate multiple signals (Table 5). Our system is expected to be independent of any generative model, compression/transmission artifact, and content-related influence: *a robust and generalized FakeCatcher, based on the essence of temporal consistency and spatial coherence of biological signals in authentic videos*. Our experimental results conclude on the following implicit formulation,

$$\begin{aligned} f = & F_1(log(D_C)) \cup \\ & F_3(log(S) \cup A_p(D_C)) \cup \\ & F_4(log(S) \cup A_p(D_C)) \cup \\ & \mu\hat{A}(S) \cup max(\hat{A}(S)) \end{aligned}$$

where we gathered 126 features combining F_1, F_3, F_4 sets, on log transforms, pairwise cross spectral densities, and spectral autocorrelations, of single source S and multi-source D_C signals. The SVM classifier trained with these 126 features on the FF dataset results in 75% accuracy. We also perform the same experiment on our Deep Fakes Dataset (with a 60/40 split) obtaining an accuracy of 76.78%.

4.3 Probabilistic Video Classification

As we coulAs mentioned in Section 3.1, the videos are split into ω-interval segments for authenticity classification. Considering that our end goal is to classify videos, we aggregate the segment labels into video labels by majority voting. Majority voting increases the segment classification accuracy of 75% to 78.18% video classification accuracy within Face Forensics dataset, hinting that some hard failure segments can be neglected due to significant motion or illumination changes. Consequently, a weighted voting scheme compensates the effect of these erroneous frames. In order to achieve that, we need the class confidences instead of discrete class labels, thus we convert our SVM to a support vector regression (SVR). Instead of a class prediction of SVM, SVR allowed us to learn the probability of a given segment to be real or synthetic. We use the expectation of the probabilities as the true threshold to classify authenticity. Also, if there is a tie in majority voting, we weigh it towards the the expectation. Using the probabilistic video classification, we increase the video classification accuracy to 82.55% in Face Forensics and to 80.35% in Deep Fakes Dataset.

4.4 CNN-based Classification

Investigating the failure cases of our probabilistic authenticity classifier, we realize that our misclassification rate of marking real segments as synthetic segments (false positive, FP) is higher than our misclassification rate of marking synthetic segments as real segments (false negative, FN). The samples ending up as false positives contain artifacts that corrupt PPG signals, such as camera movement, motion and uneven illumination. In order to improve the resiliency against such artifacts, we postulate that we can exploit the coherence of signals by increasing the number of regions of interests (ROIs) within a face. We hypothesize that coherence will be more strongly observed in real videos, as artifacts tend to be localized into specific regions in the face. However packing more signals will exponentially grow the already complex feature space (Section 6.4) for our authenticity classifier. Therefore, we switch to a CNN-based classifier, which is more suitable for a higher-dimensional segment classification task (Figure 5).

4.4.1 PPG Maps

Similar to Section 4.2, we extract C_M signals from the mid-region of faces, as it is robust against non-planar rotations. To generate same size subregions, we map the non-rectangular region of interest (ROI) into a rectangular one using Delaunay Triangulation [90], therefore each pixel in the actual ROI (each data point for C_M) corresponds to the same pixel in the generated rectangular image. We then divide the rectangular image into 32 same size sub-regions. For each of these sub-regions, we calculate $C_M = \{C_{M_0}, \ldots, C_{M_\omega}\}$, and normalize them to $[0, 255]$ interval. We combine these values for each sub-region within ω frame segment into an $\omega \times 32$ image, called PPG map, where each row holds one sub-region and each column holds one frame. Example real and synthetic PPG maps are shown in Figure 6, in the first two rows.

4.4.2 Learning Authenticity

We use a simple three layer convolutional network with pooling layers in between and two dense connections at the end (Figure 5). We use ReLU activations except the last layer, which is a sigmoid to output binary labels. We also add a dropout before the last layer to prevent overfitting. We do not perform any data augmentation and feed PPG maps directly. Our model achieves 88.97% segment and 90.66% video classification accuracy when trained on FF train set and tested on the FF test set with $\omega = 128$. Similarly, our model obtains 80.41% segment and 82.69% video classification accuracy when trained on our Deep Fakes Dataset with a random split of $60/40$.

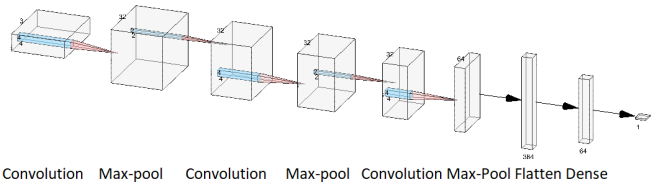

Fig. 5: **CNN Architecture.** Three convolutional layers with max pooling, followed by dense layers.

4.4.3 Spectral PPG Maps

As it is discussed in Section 3.3, frequency domain also holds important consistency information for detecting authentic content. Thus, we enhance our PPG maps with the addition of encoding binned power spectral densities $P(C_M) = \{P(C_M)_0, \ldots, P(C_M)_\omega\}$ from each sub-region, creating $\omega \times 64$ size images. Examples of our real and synthetic spectral PPG maps are shown in the last two rows of Figure 6. This attempt to exploit temporal consistency improves our accuracy for segment and video classification to 94.26% and 96% in Face Forensics, and

87.42% and 91.07% in Deep Fakes Dataset. Further classification results on different datasets are reported in Tables 15 and 10, such as 91.50% on Celeb-DF, 94.65% on FF++, and 97.36% on UADFV.

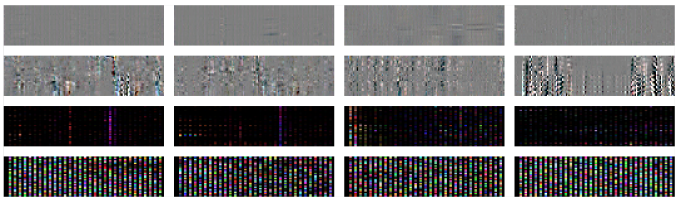

Fig. 6: **PPG Maps**. PPG signals per sub-region per frame are converted into 128×32 images for five synthetic (top) and original (bottom) segments.

5 Results

Our system utilizes Matlab [91] for signal processing, Open Face library [92] for face detection, libSVM [93] for the classification experiments, Wavelab [94] for Wavelet transformation and F_5 feature set, and Keras [95] for network implementations. In this section, we first describe the benchmark datasets and introduce our new Deep Fakes Dataset. Then we examine some parameters of the system, such as the facial regions of signals in S, segment durations ω, and dimensionality reduction techniques on the feature set F. We also compare our system against other detectors, demonstrate that our system is superior to complex baseline architectures, and summarize our experimental outcomes.

5.1 Deep Fakes Dataset

The external datasets we used are explained in Section2.5. Although FF is a clean dataset perfect for initial experiments, we need to assess the generalizability of our findings. For this purpose, we created a new database (so-called Deep Fakes Dataset (DF)), which is a set of portrait videos collected "in the wild". The videos in our dataset are diverse real-world samples in terms of the source generative model, resolution, compression, illumination, aspect-ratio, frame rate, motion, pose, cosmetics, occlusion, content, and context, as it originates from various sources such as media sources, news articles, and research presentations; totaling up to 142 videos, 32 minutes, and 30 GBs. For each synthetic video, we searched for the original counterpart if it is not presented with its source. For example, if a synthetic video is generated from a movie, we found the real movie and cropped the corresponding segment. When we could not locate the source, we included a similar video to preserve the class balance (i.e., for a given fake award speech, we included a similar (in size, location, and length) original award speech). This variation does not only increase the diversity of our synthetic samples, but it also makes our dataset more challenging by breaking possible real-fake associations.

Figure 7 demonstrates a subset of the Deep Fakes Dataset, original videos placed in the top half and fakes in the bottom half. A small clip consisting of several videos in the dataset can also be found in the Supplemental Material. The dataset is publicly released for academic use[1]. High accuracy on Deep Fakes Dataset substantiates that FakeCatcher is robust to low-resolution, compression, motion, illumination, occlusion, pose, and cosmetics artifacts; that enrich the input and slightly reduce the accuracy, without preprocessing. We also perform cross-dataset evaluations which support our aforementioned claims about generalizability.

1. http://bit.ly/FakeCatcher

Fig. 7: **Deep Fakes Dataset.** We introduce a diverse dataset of original (top) and fake (bottom) video pairs from online sources.

5.2 Evaluations

We conduct several evaluations to establish our approach as state-of-the-art solution for deep fake detection. First, we justify the use of biological signals by several comparisons to off the shelf deep learning solutions and to other fake detectors. Second, we list several crucial experiments to guide us in the combinatorial signal-feature space. Third, we summarize and relate our experimental findings to each result experiment section.

5.2.1 *Quantitative Comparisons*

In order to promote the effect of biological signals on the detection rate, we perform some experiments with several networks: (i) a simple CNN, (ii) Inception V3 [96], (iii) Xception [97], (iv) ConvLSTM [98], (v-vii) three best networks proposed in [45], and (viii) our approach.

Model	Frame	Face	Video
Simple CNN	46.89%	54.56%	48.88%
InceptionV3	73.85%	60.96%	68.88%
Xception	78.67%	56.11%	75.55%
ConvLSTM	47.65%	44.82%	48.83%
[45] V1	**86.26%**	-	82.22%
[45] V3	76.97%	-	73.33%
[45] ensemble	83.18%	-	80.00%
Ours	-	**87.62%**	**91.07%**

TABLE 6: **Comparison.** Detection accuracies of several networks trained on images, face images, and videos. The next best after our approach is 8.85% less accurate.

All experiments in Table 6 are performed on the same 60% train and 40% test split of our Deep Fakes Dataset, with same meta parameters. We choose to compare on Deep Fakes Dataset, because it is more generalizable as discussed in the previous section. For ConvLSTM and our approach, "Frame" and "Face" indicate segment accuracy, for others they indicate frame accuracy.

The last column is video accuracy (Section 4.3). We did not run [45] on face images because their approach utilizes background, and we did not run ours on entire frames because there is no biological signal in the background. We emphasize that **FakeCatcher outperforms the best baseline architecture by 8.85%**.

5.2.2 Qualitative Comparisons

Even though "deep fakes" is a relatively new problem, there are a few papers in this domain. [2] employs a generative model for detection, but their model is restricted to their generative method in [37]. [20] also claims a high detection rate if the synthetic content is generated by [37] or the VAE used in the *FakerApp*. [22] reports high accuracy, however their approach is dependent on eye detection and parameterization. All of these [2], [20], [45] employ neural networks blindly and do not make an effort to understand the generative noise that we experimentally characterized using biological signals (Section 5.2.4).

Based on our comprehensive experiments, we observe that biological signals are not well-preserved in deep fakes (Section 3.3), however, *is the contribution of biological signals significant against pure ML approaches*? We claim that PPG maps encode authenticity using their spatial coherence and temporal consistency. To prove this, we train the CNN in Section 4.4.2 with (i) input frames (46.89%), (ii) faces cropped from input frames (54.56%), and (iii) our PPG Maps (Section 4.4) (87.62%) as shown in Table 6. The significant accuracy increase justifies the use of biological signals. To ensure that this jump is not only the result of temporal consistency, we compare it to the classification accuracy of ConvLSTM on entire and face frames (47.65% and 44.82%), which are even lower than frame-based methods. Thus, we certify that (1) *approaches incorporating biological signals are quantitatively more descriptive for deep fake detection compared to pure machine learning based approaches*, (2) *both spatial and temporal properties of biological signals are important*, and (3) *these enable our network to perform significantly better than complex and deeper networks*.

5.2.3 Validation Experiments

We experimentally validate the combination of signals and feature sets used throughout the paper, namely 6 signals, in 11 transformations, in 126 features; explored in over 70 experiments. We document all experiments with the signal transformation (Table 3), feature set (Table 4), and SVM classification accuracy, trained on FF (Table 8) and on DF datasets (Table 7), with $\omega = 128$. Furthermore, in Table 9, we document experiments where we selected specific subsets of Face Forensics (FFT for train, FFX for test, and FFC for validation sets).

5.2.4 Summary of Experimental Outcomes and Findings

- **Spatial coherence:** Biological signals are not coherently preserved in different synthetic facial parts.
- **Temporal consistency:** Synthetic content does not contain frames with stable PPG. $\hat{A}$ and P of PPGs significantly differ. However, inconsistency is not separable into frequency bands (Section 6.6.3).
- **Combined artifacts:** Spatial inconsistency is augmented by temporal incoherence (Experiments in $5.2.3(S_C)$).
- **Artifacts as features:** These artifacts can be captured in explainable features by transforming biological signals (Section 5.2.3, and Tables 2,3&4). However there exists no clear reduction of these feature sets into lower dimensions (Section 6.4), thus CNN performs better than SVM.
- **Comprehensive analysis:** Finally, our classifier has higher accuracy for detection in the wild, for shorter videos, and for mid-size ROIs (Section 6).

Feature set	Signal	# features	Accuracy
F_6	S	600	43.22
F_{12}	S	12	43.41
F_3	log(S)	24	43.81
F_6	log(S)	600	43.81
F_{12}	S	12	43.61
F_3	S	24	45.57
F_4	log(S)	36	48.13
F_7	S	30	48.52
$F_4F_3F_1$ F_4F_3	$log(S)$x2,$log(D_C)$, $A_p(log(D_C))$	96	54.02
F_5	S	767	54.22
$\mu()max()$	$A(log(S))$	12	54.22
F_7	log(S)	30	55.40
F_5	S	390	58.84
F_5	A(log(S))	390	60.90

TABLE 7: **Classification Results on DF.** Accuracies with $\omega = 128$, on DF dataset, and train/test split of 60/40.

Feature Set	Signal	#Feat.	Acc
F_5	S	774	51.23
F_8	$log(S)$	18	51.81
F_6	$log(S)$	600	51.89
F_7	S	30	58.06
F_7	S_C	15	59.29
$\mu(A_p()))$	$log(D)$	3	62.3
F_2	$log(S)$	78	64.04
F_2	$log(S_C)$	39	64.32
F_3, F_3	$\hat{A}(S)$,13	36	64.89
F_5	$log(S)$	768	65.27
F_1	$C_L - C_R$	2	65.37
F_1	$C_L - C_M$	2	65.55
F_7	$log(S)$	30	65.55
F_1	$C_M - C_R$	2	65.84
F_5	S_C	768	66.03
F_6	$\hat{A}(S)$	600	66.03
F_2	S_C	39	66.88
$\mu(A()))$	S_C	3	66.88
$\mu(A_p()))$	$log(D_C)$	3	66.88
F_5	$A_p(log(D_C))$	384	66.92
F_1	$log(D_C)$	6	67.17
F_6	S_C	300	67.26
F_3	$log(S)$	24	67.55
F_3F_3	$A_p(log(D_C))$,$\hat{A}(S)$	36	67.55
$F_4F_3\mu()$	$A_p(S)$	63	68.12
$\mu()$	$A(log(S))$	6	68.88
F_6	$log(S)$	600	69.04
F_4	$log(S)$	36	69.07
F_2	S	78	69.26
F_5	$P(W(S))$	390	69.63
$\mu()$	$A_p(log(D_C))$,$A(log(S))$	9	69.63
$F_1F_2F_3F_4F_5$ $F_5F_6F_7F_{12}$	$log(D_C)$,S,$log(S)$x2, $log(S)$x2,S,$log(S)$x2	1944	70.49
$F_4F_3\mu()$	$log(S)$x2,$A_p(D_C)$	63	71.34
$F_4F_3F_1$ F_4F_3	$log(S)$x2,$log(D_C)$, $A_p(log(D_C))x2$	96	72.01

TABLE 8: **Classification Results on FF.** Accuracies of signal transformations and corresponding feature sets.

5.3 Cross Dataset/Model Experiments

We experiment by training and testing on (i) different datasets, and (i) datasets created by different generative models for the

evaluation of our approach. Our cross dataset experiments are conducted between Deep Fakes (ours), Celeb-DF [4], FF [2], FF++ [3], and UADFV [56] datasets where we train our proposed approach on one dataset and test on another (Table 10). Based on rows 5 and 6, the key observation is that FakeCatcher learns better from small and diverse datasets than on large and single source datasets. On one hand, training on DF and testing on FF is 18.73% higher than the other way around. On the other hand, DF is approximately only 5% of FF. The main difference between these datasets is that FF has a single generative model with no other artifacts, and DF is a completely in-the-wild dataset. If we compare rows 3 and 6, we also observe that increasing diversity from FF to FF++, increases the accuracy on DF by 16.9%.

Train	Test	Video Accuracy
Celeb-DF [4]	FF++ [3]	83.10%
FF++ [3]	Celeb-DF [4]	86.48%
FF++ [3]	Deep Fakes Dataset	84.51%
Celeb-DF [4]	Deep Fakes Dataset	82.39%
Deep Fakes	FF [2]	86.34%
FF [2]	Deep Fakes Dataset	67.61%
FF++ [3]	UADFV [56]	97.92%
Deep Fakes Dataset	FF++ [3]	80.60%
Deep Fakes Dataset	Celeb-DF [4]	85.13%

TABLE 10: **Cross Dataset Results.** Accuracies for FakeCatcher trained on the first column and tested on the second column.

As mentioned in Section 2.5, FF++ [3] contains four synthetic videos per original video, where each of them is generated using a different generative model. First, we partition original videos of FF++ into train/test sets with 60/40 percentages. We create four copies of these sets, and delete all samples generated by a specific model from each set (column 1, Table 11, where each set contains 600 real and 1800 fake videos from three models for training, and 400 real and 400 fake videos from one model for test. Table 11 displays the results of our cross model evaluation. We obtain significantly accurate predictions, except NeuralTextures [77], as it is an inherently different generative model.

Train	Test	Video Accuracy
FF++ - Face2Face	Face2Face [37]	95.25%
FF++ - FaceSwap	FaceSwap [59]	96.25%
FF++ - Deepfakes	Deepfakes [57]	93.75%
FF++ - NeuralTextures	NeuralTextures [77]	81.25%

TABLE 11: **Cross Model Results on FF++.** Accuracies of FakeCatcher on FF++ dataset variations, where the samples generated by the model in the second column is excluded as test set.

6 ANALYSIS

As we introduce some variables into our automatic FakeCatcher, we would like to assess and reveal the best values for those parameters. Segment duration, face region, and different preprocessing techniques for PPGs are explored in our analysis section. Furthermore, we analyzed the explainable feature space for its information content and observed its reaction to dimensionality reduction techniques.

6.1 Segment Duration Analysis

Table 12 documents results on the test set, the entire Face Forensics dataset, and Deep Fakes Dataset, using different segment durations. Top half shows the effect of ω on the pairwise classification. The choice of $\omega = 300$ (10 sec) is long enough to detect strong correlations without including too many artifacts for video labels.

Preceded by probabilistic video classification, authenticity classifier can be used with different segment sizes, which we investigate in this section. Selecting a long segment size can accumulate noise in biological signals, in contrast incorrectly labeled segments may be compensated in the later step if we have enough segments. Thus, selecting a relatively smaller segment duration $\omega = 180$ (6 sec), increases the video classification accuracy while keeping it long enough to extract biological signals. Note that when we increase ω above a certain threshold, the accuracy drops for Deep Fakes Dataset. This is due to occlusion and illumination artifacts, because the segment covers more facial variety as ω increases. A correct balance of having sufficient segments versus sufficient length per segment is a crucial result of our analysis.

6.2 Face Analysis

In this section, we evaluated the dependency of our approaches on different face regions and on face detection accuracy.

6.2.1 Size of Face Regions

For our SVM classifier, biological signals are extracted from three separate regions on the face. In this section, we assess the effects of different sizes for these regions of interests. We quantize the ROIs as very small (a few pixels), small, default, big, and the

Feature set	signal	test	ω	train	# feat.	s. acc	v. acc
F_5	$G(S)$	FFX	300	FFT+FFC	300	50	-
F_6	$G(S)$	FFX	300	FFT+FFC	600	64.75	-
F_5	$G(log(S))$	FFX	300	FFT+FFC	300	70.25	
$LDA_3(F_1F_3F_4$	$log(D_C)$,$A_p(log(D_C))$x2,	FFX	300	FFT+FFC	3	71.75	-
$F_{12}F_3F_4)$	S,$log(S)$x2						-
$F_1F_3F_4F_{12}F_3F_4$	$log(D_C)$,$A_p(log(D_C))$x2,S,$log(S)$x2	FFC	300	FFT+FFX	108	71.79	-
$F_1F_3F_4\mu()F_3F_4$	$log(D_C)$,$A_p(log(D_C))$x2,$A(S)$,$log(S)$x2	FFC	128	FFT+FFX	108	72.21	-
$PCA_3(F_1F_3F_4$	$log(D_C)$,$A_p(log(D_C))$x2,	FFX	300	FFT+FFC	3	71	69.79
$F_{12}F_3F_4)$	S,$log(S)$x2						
$F_1F_3F_4F_3F_4F_5$	$log(D_C)$,$A_p(log(D_C))$x2,$log(S)$x2,S	FFX	300	FFT+FFC	1631	73.25	72.81
$F_1F_3F_4F_{12}F_3F_4$	$log(D_C)$,$A_p(log(D_C))$x2,S,$log(S)$x2	FFX	300	FFT+FFC	126	75	75.16
$F_1F_3F_4F_{12}F_3F_4$	$log(D_C)$,$A_p(log(D_C))$x2,S,$log(S)$x2	FFX	300	FFT	108	74.5	75.50
$F_1F_3F_4F_{12}F_3F_4$	$log(D_C)$,$A_p(log(D_C))$x2,S,$log(S)$x2	FFX	300	FFT+FFC	108	75	78.18
$F_1F_3F_4F_{12}F_3F_4$	$log(D_C)$,$A_p(log(D_C))$x2,S,$log(S)$x2	FFX	128	FFT	108	76.37	79.53
$F_1F_3F_4F_3F_4$	$log(D_C)$,$A_p(log(D_C))$x2,$log(S)$x2	FFX	128	FFT+FFC	108	75.51	79.53
$F_1F_3F_4F_{12}F_3F_4$	$log(D_C)$,$A_p(log(D_C))$x2,S,$log(S)$x2	FFX	128	FFT+FFC	126	77.12	81.54
$F_1F_3F_4F_{12}F_3F_4$	$log(D_C)$,$A_p(log(D_C))$x2,S,$log(S)$x2	FFX	128	FFT+FFC	108	**77.50**	**82.55**

TABLE 9: **Classification on mixed train/test sets:** We evaluate FakeCatcher on several subsets, with various signals and features.

ω	dataset	s. acc.	v. acc.	CNN s.	CNN v.
64	FF test	95.75%	-	-	-
128	FF test	96.55%	-	-	-
256	FF test	98.19%	-	-	-
300	FF test	**99.39%**	-	-	-
64	FF	93.61%	-	-	-
128	FF	94.40%	-	-	-
256	FF	94.15%	-	-	-
300	FF	**95.15%**	-	-	-
128	DF	75.82%	78.57%	**87.42%**	**91.07%**
150	DF	73.30%	75.00%	-	-
180	DF	**76.78%**	**80.35%**	86.25%	85.71%
240	DF	72.17%	73.21%	-	-
300	DF	69.25%	66.07%	-	-
128	FF	**77.50%**	**82.55%**	**94.26%**	**96%**
150	FF	75.93%	78.18%	-	-
180	FF	75.87%	78.85%	92.56%	93.33%
256	FF	72.55%	73.82%	-	-
300	FF	75.00%	75.16%	-	-
450	FF	70.78%	71.33%	-	-
600	FF	68.75%	68.42%	-	-

TABLE 12: **Accuracy per Segment Duration.** Effects of ω, on segment and video accuracies, using SVM and CNN classifiers, on FF test, entire FF, and DF datasets. First 8 rows denote pairwise task.

ROI	# pix	data	ω	# seg	p. acc	s. acc	v. acc
Smallest	356	FF	128	1058	95.46	68.25	70.33
Smallest	356	FF	300	400	98.50	68.18	67.79
Smallest	356	DF	128	140	68.76	59.44	55.55
Smallest	356	DF	300	43	60.51	61.36	60.86
Small	2508	FF	128	1058	93.00	**80.94**	81.51
Small	2508	FF	300	400	94.50	77.41	76.47
Small	2508	DF	128	140	80.35	61.53	60.00
Small	2508	DF	300	43	81.53	68.18	65.21
Default	7213	FF	128	1058	96.55	77.50	**82.55**
Default	7213	FF	300	400	**99.39**	75.00	75.16
Default	7213	DF	128	140	83.55	**75.82**	**78.57**
Default	7213	DF	300	43	**83.69**	69.25	66.07
Big	10871	FF	128	1058	84.87	74.75	77.50
Big	10871	FF	300	400	87.50	73.07	71.66
Big	10871	DF	128	140	78.58	63.57	63.63
Big	10871	DF	300	43	82.51	60.46	59.09
Face	10921	FF	128	1058	61.66	60.04	74.23
Face	10921	FF	300	400	58.97	60.00	74.84
Face	10921	DF	128	140	58.93	61.53	62.22
Face	10921	DF	300	43	56.97	50.00	52.17

TABLE 13: **ROI Analysis on SVM Classifier:** Five different ROI sizes are evaluated on FF and DF datasets, with different segment sizes. Corresponding values are plotted in Figure 9, and corresponding ROI's are drawn on Figure 8.

whole face. Table 13 documents experiments with these ROIs, their corresponding number of pixels, dataset, segment duration ($\omega = 128$ and for $\omega = 300$), and number of segments, with resulting accuracies for pairwise, segment, and video tasks. We also plot the pairwise separation, segment classification, and video classification accuracies per ROI size, on two datasets in Figure 9. Lastly, we show these ROIs on a sample video frame in Figure 8, where red contour corresponds to G_L and C_L, green to G_M and C_M, and blue to G_R and C_R. We conclude that our default ROI is a generalizable choice with a good accuracy for all cases.

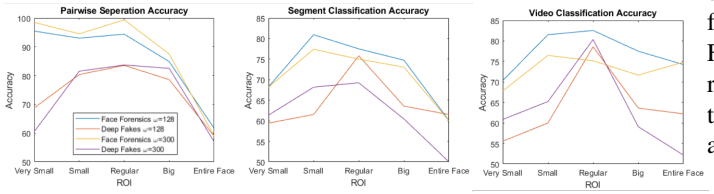

Fig. 9: **ROI Comparison.** Pairwise separation (left), segment (middle), and video (right) classification accuracy per several ROIs, on FF and DF datasets.

6.2.2 *Face Detection Dependency*

Our method needs some skin to extract biological signals. We do not need a perfect face detector, however we need to find some facial area to extract the signal. Our implementation is modular enough to enable using other face detectors and handle multiple faces, both of which affects the accuracy but not significantly. In order to assess our robustness against face detection accuracy, we demonstrate results where (i) the face detection accuracy is very low, and (ii) the video has multiple faces.

In Figure10, our results on unmodified but edge-case videos are shown. The top video contains two faces, we process them separately and we find each of them to be fake, with an average confidence of 91.7%. On the left is a fake video, even though its face detection accuracy is 3% (very low compared to the average), FakeCatcher classifies this video as fake with 99.97%. Lastly, the real video on the right has a significant frame ordering problem, thus the face detector has 17% accuracy. Nevertheless we classify as real with 65%.

6.3 Image Quality Analysis

In order to estimate an exact heart rate, the PPG signal needs to have very low SNR. In contrast, the spatio-temporal inconsistency of PPGs is sufficient for our approach to detect fakes. Even low quality authentic videos can still preserve this consistency,

Fig. 8: **ROI Contours.** Whole face (a), big ROI (b), default (c), small ROI (d), few pixels (e), for G_L and C_L (blue), for G_M and C_M (green), and for G_R and C_R (red).

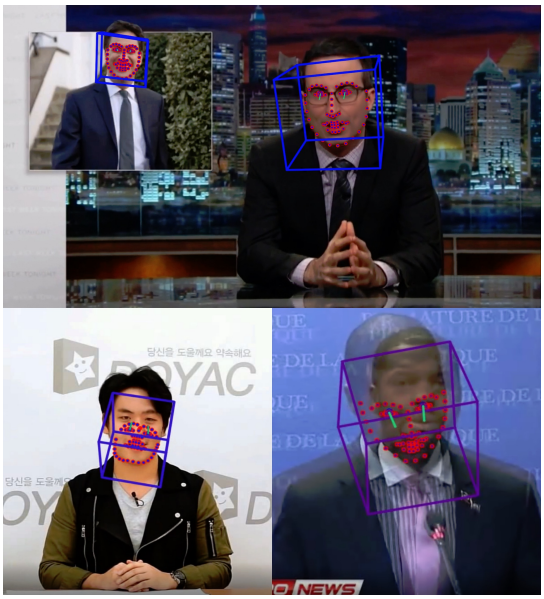

Fig. 10: **Face Detection Dependency.** FakeCatcher catches a fake video with multiple faces (top) as 91.7% fake, a fake video with 3% face detection confidence (left) as 99.97% fake, and a real video with 17% face detection confidence (right) as 65.47% real.

differentiating our dependency on low noise condition compared to the heart rate estimation task. To support this postulation, we analyze our detection accuracy with images processed with two commonly used image processing operations: Gaussian blur and median filtering. We use Celeb-DF [4] dataset, with different kernel sizes, fixing $\omega = 128$ segment duration (Table 14). The accuracy stays relatively unaffected up to a kernel size of 7x7. Then, as expected, the larger the filter kernel is used, the lower the accuracy gets. Nevertheless, such large kernel blurs modify the image significantly enough that it does not matter if the image is authentic or fake (Figure 11).

Operation	Kernel	Accuracy
Original	N/A	91.50%
Gaussian blur	3x3	91.31%
Gaussian blur	5x5	88.61%
Gaussian blur	7x7	85.13%
Gaussian blur	9x9	70.84%
Gaussian blur	11x11	65.44%
Median Filter	3x3	88.41%
Median Filter	5x5	83.01%
Median Filter	7x7	71.42%
Median Filter	9x9	65.44%
Median Filter	11x11	65.25%

TABLE 14: **Robustness.** FakeCatcher accuracies on Celeb-DF dataset under different Gaussian Blur and Median filtering operations with different kernel sizes.

Fig. 11: **Robustness.** Original (left) and blurred images with 7x7 (middle) and 11x11 (right) kernels.

6.4 Blind Source Separation

To better understand our features, feature sets, and their relative importance, we computed the Fisher criterion detection [99] of linearly separable features if we have any. No significantly high ratio was observed, neither for LDA (linear discriminant analysis) [100], guiding us towards kernel based SVMs and more feature space exploration. We also applied PCA (principal component analysis) [101] and CSP (common spatial patterns) [102] to reduce the dimensionality of our feature spaces. Figure 12 shows 3D distribution of original (red) and synthetic (blue) samples by the most significant three components found by PCA, LDA, and CSP, without clear class boundaries. We also tried to condense the feature vector with our best classification accuracy. However, we achieved 71% accuracy after PCA and 65.43% accuracy after CSP.

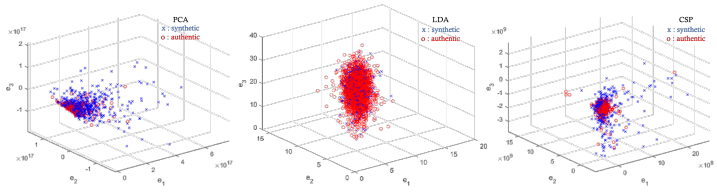

Fig. 12: **Feature Space.** Original (red) and synthetic (blue) samples in three dominant component space, extracted using PCA (left), LDA(mid), and CSP (right).

6.5 Class Accuracies

Throughout our paper, we use the metric as dataset accuracy in order to simplify the explanation of results. However, catching fake videos (true positives) is as important as passing real videos through (true negatives). In some defensive systems, detecting real videos as fake (false positive) is more tolerable than letting fake videos slip (false negatives), because there is a secondary manual detection process. On the other hand, too many false positives may overwhelm the system towards manually checking everything.

In order to assess our system towards these concerns, we analyzed the class accuracies of FakeCatcher in different datasets. Table15 lists all dataset, real, and synthetic accuracies on all datasets used throughout the paper, and with specific generative models of FF++ [3]. All models use $\omega = 128$ and a 60/40 split, except the one trained on Celeb-DF using the given subsets. We observe that there is a slight general tendency of creating false positives. We also note the special case of Celeb-DF that its class imbalance of 6.34:1 fake to real ratio bumps up this tendency. We claim that this disturbance is the side effect of the head motion, lighting, color artifacts, and other environment changes on the PPG signal. However, our probabilistic video classification, incorporating frequency domain, and appropriate segment durations negate these side effects. Following the discussion in the beginning of this section, we believe that automatic monitoring systems would prefer false positives over false negatives as long as it is not overwhelming the secondary manual process; which makes FakeCatcher a good candidate for deployment to production.

6.6 Signal Processing Enhancements

In this subsection, we document the representativeness of several possible pre/post processing of feature sets and signals by small experiments while keeping the signal and feature set the same.

Dataset	Gen. Model	%Dataset	%Real	%Synthetic
UADFV [56]	FakeApp [75]	97.36%	94.93%	100%
FF++ [3]	Face2Face [37]	96.37%	96.00%	96.75%
FF [2]	Face2Face [37]	96%	94.24%	97.75%
FF++ [3]	FaceSwap [59]	95.75%	94.75%	96.75%
FF++ [3]	Deepfakes [57]	94.87%	93.25%	96.50%
FF++ [3]	All	94.65%	88.25%	96.25%
Celeb-DF [4]	Default	91.50%	76.40%	99.41%
DF (ours)	Mixed	91.07%	85.26%	96.89%
FF++ [3]	Neural Textures [77]	89.12%	86.75%	91.50%

TABLE 15: **Class Accuracies.** Accuracies per dataset, per source, and per class, on FF, DF, FF++, and Celeb-DF.

6.6.1 Normalization

We evaluated the most representative pairwise segmentation result (Section 3.3) with different normalizations on the signals before computing their cross power spectral densities (Table 16). We used the same toy FF dataset and kept $\omega = 300$ constant, producing 387 segments. In this specific separation task, this analysis demonstrated that all frequencies and their ranges are needed as normalization may remove some characteristics of the signals to differentiate original and fake signals.

Normalization	Accuracy
None	**99.39**
2-norm	87.34
∞-norm	84.03
Standardized moment	63.55
Feature scaling	59.03
Spectral whitening	49.09
Coefficient of variation	34.03

TABLE 16: **Normalization Effects:** Several normalization techniques are applied to the best configuration in the pairwise test.

6.6.2 Band Pass Filtering

We also analyzed if different frequency bands contributed in the generative noise. We divided the spectrum into below ($f < 1.05$Hz), acceptable ($1.05\text{Hz} < f < 3.04\text{Hz}$), and high heart rate frequency bands ($3.04\text{Hz} < f < 4.68\text{Hz}$) as well as an additional high frequency band ($f > 4.68$Hz). Table 17 documents pairwise separation accuracies of the most representative feature, for segment size $\omega = 300$ on entire FF dataset (1320 segments).

Frequency band	Accuracy
0-15	**95.15**
0-1.05	80.58
1.05-3.04	88.51
3.04-4.68	88.21
4.68-15	94.92

TABLE 17: **Frequency Bands:** Analysis on several frequency bands for best pairwise separation accuracy on entire FF dataset.

6.6.3 Frequency Quantization

We also analyzed the effect of quantization after taking the inverse Fourier Transform of the signal. In Table 18 we verified that 256 bins were the optimum choice on the best configuration discussed in Section 3.3 in the main paper, on the entire FF dataset.

6.6.4 DCT Coefficients as Features

We experimented with using DCT of the signal (C_M in this case) up to $N = \{1, 2, 3, 4\}$ elements as a feature set, however the accuracy was surpassed as shown in the Section 5.2.3. The settings below in Table 19 correspond to the summation of DCT values up to N, respectively.

iFFT bins	Accuracy
64	94.01
128	94.92
256	**95.15**
512	94.92

TABLE 18: **Quantization Evaluation:** Analysis on different bin counts for best pairwise separation accuracy on entire FF dataset.

ω	#videos	Setting	Accuracy	Setting	Accuracy
512	62	D	70.96	B	77.41
256	236	D	70.33	B	72.03
196	323	D	71.20	B	77.39
128	532	D	68.23	B	72.93
64	1153	D	65.04	B	69.64
512	62	C	75.80	A	77.41
256	236	C	67.18	A	73.72
196	323	C	77.39	A	75.54
128	532	C	73.30	A	73.68
64	1153	C	68.08	A	69.55

TABLE 19: **DCT Components as Features:** Following some image spoofing papers, we evaluated accuracies with several DCT cut-offs with several segment sizes.

7 Implementation Details

For each segment, we apply Butterworth filter [79] with frequency band of $[0.7, 14]$. We quantize the signal using Welch's method [103]. Then, we collect frequencies between $[h_{low}, h_{high}]$, which correspond to below, in, and high ranges for heart beat. There is no clear frequency interval that accumulated generative noise, so we include all frequencies. We follow the PPG extraction methods in [71] for G_L, G_M, G_R and [70] for C_L, C_M, C_R.

It is worth discussing that PPG signals extracted for heart rate and for our detection task are not of the same quality. For accurate heart rate estimation, PPG signal goes through significant denoising and componentization steps to fit the signal into expected ranges and periods. We observe that some signal frequencies and temporal changes that may be considered as noise for heart rate extraction actually contains valuable information in terms of fake content. For our task, we only utilize their coherence among facial regions and their consistency across segments, achieving 99.39% pair separation accuracy on Face Forensics. Therefore, we intentionally did not follow some steps of cleaning the PPG signals with the motivation of keeping subtle generative noise. Also, we attest that even though videos undergo some transformations (e.g., illumination, resolution, and/or compression), raw PPG correlation does not change in authentic videos.

8 Future Work

Our main focus in this paper is portrait videos, for which deep fakes are the most harmful. For general fake videos without humans, one possible extension of our work is to discover formulations of other spatiotemporal signals (i.e., synthetic illumination, wind) that can be faithfully extracted from original videos.

For FakeCatcher, we see room for improvement by proposing a more complex CNN architecture. However, we want to go further and develop a "BioGAN" that explores the possibility of

a biologically plausible generative model. Mimicking biological signals may be possible by introducing an extra discriminator whose loss incorporates our findings to preserve biological signals. This necessitates the extraction process to be approximated with a differentiable function in order to enable backpropagation. The development of BioGAN puts an expiration date on this work, however formulating a **differentiable** loss function that follows the proposed signal processing steps is not straightforward.

The dataset structure is another discussion we would like to pose for forthcoming research. For the generalizability of a detector, the data should not be biased towards known generative models. Another layer of complication which we would like to further investigate is learning from random fake and real video pairs (similar to [46] and partially to our dataset). In our work, this conceals the actual features we want to learn, thus decreasing the accuracy for the "in the wild" case. Learning from pairs enables us to reduce the effects of other variants and makes the model focus on the generative differences, even though there is compression, motion, illumination artifacts. All pure machine learning based algorithms (as shown in Table 6) have a drop in accuracy compared to ours due to blindly exploiting this generative noise. On the other hand, we investigate the projection of this noise in biological signal domain, as a more descriptive interpretation, enabling our approach to outperform deeper models.

9 Conclusion

In this paper, we present FakeCatcher, a fake portrait video detector based on biological signals. We experimentally validate that spatial coherence and temporal consistency of such signals are not well preserved in GAN-erated content. Following our statistical analysis, we are able to create a robust synthetic video classifier based on physiological changes. Furthermore, we encapsulate those signals in novel PPG maps to allow developing a CNN-based classifier, which further improves our accuracy and is agnostic to any generative model. We evaluate our approach for pairwise separation and authenticity classification, of segments and videos, on Face Forensics [2] and newly introduced Deep Fakes Dataset, achieving 99.39% pairwise separation accuracy, 96% constrained video classification accuracy, and 91.07% in the wild video classification accuracy. These results also verify that FakeCatcher detects fake content with high accuracy, independent of the generator, content, resolution, and quality of the video.

Apart from the FakeCatcher and the Deep Fakes Dataset, we believe that a main contribution of this paper is to provide an in-depth analysis of deep fakes in the wild. To our knowledge, generative models are not explored by biological signals before, and we present the first experimental study for understanding and explaining human signals in synthetic portrait videos. We hope that our findings will illuminate the future research in defense against deep fakes. Lastly, we encourage continuation of generalizable fake detection research by making our Deep Fakes Dataset available to the research community.

Acknowledgments

We would like to thank Prof. Daniel Aliaga for proofreading an earlier version of the manuscript. We would also like to thank for the supportive research environments in the authors' current and previous institutions, and funding resources as NSF (CNS-1629898), Center of Imaging, Acoustics, and Perception Science, and the Research Foundation of Binghamton University. Lastly, we would like to acknowledge the reviewers' constructive feedback towards improving the experimental evaluation and the clarity of our approach.

References

[1] D. Chu, I. Demir, K. Eichensehr, J. G. Foster, M. L. Green, K. Lerman, F. Menczer, C. OConnor, E. Parson, L. Ruthotto *et al.*, "White paper: Deep fakery – an action plan," Institute for Pure and Applied Mathematics (IPAM), University of California, Los Angeles, Los Angeles, CA, Tech. Rep. http://www.ipam.ucla.edu/wp-content/uploads/2020/01/Whitepaper-Deep-Fakery.pdf, Jan. 2020.

[2] A. Rössler, D. Cozzolino, L. Verdoliva, C. Riess, J. Thies, and M. Nießner, "FaceForensics: A Large-scale Video Dataset for Forgery Detection in Human Faces," *arXiv*, p. arXiv:1803.09179, Mar 2018.

[3] A. Rossler, D. Cozzolino, L. Verdoliva, C. Riess, J. Thies, and M. Niessner, "Faceforensics++: Learning to detect manipulated facial images," in *The IEEE International Conference on Computer Vision (ICCV)*, October 2019.

[4] Y. Li, P. Sun, H. Qi, and S. Lyu, "Celeb-DF: A Large-scale Challenging Dataset for DeepFake Forensics," in *IEEE Conf. on Computer Vision and Patten Recognition (CVPR)*, Seattle, WA, United States, 2020.

[5] I. Goodfellow, J. Pouget-Abadie, M. Mirza, B. Xu, D. Warde-Farley, S. Ozair, A. Courville, and Y. Bengio, "Generative adversarial nets," in *Advances in Neural Information Processing Systems 27*. Curran Associates, Inc., 2014, pp. 2672–2680.

[6] A. Radford, L. Metz, and S. Chintala, "Unsupervised Representation Learning with Deep Convolutional Generative Adversarial Networks," *arXiv e-prints*, p. arXiv:1511.06434, Nov 2015.

[7] J.-Y. Zhu, T. Park, P. Isola, and A. A. Efros, "Unpaired image-to-image translation using cycle-consistent adversarial networks," in *Computer Vision (ICCV), 2017 IEEE International Conference on*, 2017.

[8] T.-C. Wang, M.-Y. Liu, J.-Y. Zhu, G. Liu, A. Tao, J. Kautz, and B. Catanzaro, "Video-to-video synthesis," in *Advances in Neural Information Processing Systems (NIPS)*, 2018.

[9] K. Nagano, J. Seo, J. Xing, L. Wei, Z. Li, S. Saito, A. Agarwal, J. Fursund, and H. Li, "pagan: Real-time avatars using dynamic textures," *ACM Transactions on Graphics*, 2018.

[10] A. Pumarola, A. Agudo, A. Martinez, A. Sanfeliu, and F. Moreno-Noguer, "Ganimation: Anatomically-aware facial animation from a single image," in *Proceedings of the European Conference on Computer Vision (ECCV)*, 2018.

[11] Y. Li, S. Liu, J. Yang, and M.-H. Yang, "Generative face completion," in *IEEE Conference on Computer Vision and Pattern Recognition*, 2017.

[12] "Fake obama warning about 'deep fakes' goes viral," https://www.msnbc.com/hallie-jackson/watch/fake-obama-warning-about-deep-fakes-goes-viral-1214598723984, accessed: 2020-03-15.

[13] "Fake celebrity porn is blowing up on reddit, thanks to artificial intelligence," https://www.theverge.com/2018/1/24/16929148/fake-celebrity-porn-ai-deepfake-face-/swapping-artificial-intelligence-reddit, accessed: 2018-11-15.

[14] "Deep fakes: A looming crisis for national security, democracy and privacy?" https://www.lawfareblog.com/deep-fakes-looming-crisis-national-/security-democracy-and-privacy, accessed: 2018-11-15.

[15] "Ai art at christies sells for $432,500," https://www.nytimes.com/2018/10/25/arts/design/ai-art-sold-christies.html, accessed: 2018-11-15.

[16] J. Benes, T. Kelly, F. Dechtverenko, J. Krivanek, and P. Müller, "On realism of architectural procedural models," *Computer Graphics Forum*, vol. 36, no. 2, pp. 225–234, May 2017.

[17] J. Pan, J. Dong, Y. Liu, J. Zhang, J. Ren, J. Tang, Y. W. Tai, and M.-H. Yang, "Physics-based generative adversarial models for image restoration and beyond," *IEEE Transactions on Pattern Analysis and Machine Intelligence*, 2020.

[18] L. Scalise, N. Bernacchia, I. Ercoli, and P. Marchionni, "Heart rate measurement in neonatal patients using a webcamera," in *2012 IEEE International Symposium on Medical Measurements and Applications Proceedings*, May 2012, pp. 1–4.

[19] M. Rostami, A. Juels, and F. Koushanfar, "Heart-to-heart (h2h): authentication for implanted medical devices," in *Proceedings of the 2013 ACM SIGSAC Conference on Computer and Communications Security*, ser. CCS '13. New York, NY, USA: ACM, 2013, pp. 1099–1112.

[20] D. Afchar, V. Nozick, J. Yamagishi, and I. Echizen, "Mesonet: a compact facial video forgery detection network," in *IEEE International Workshop on Information Forensics and Security (WIFS)*, Dec 2018, pp. 1–7.

[21] S. Agarwal, H. Farid, Y. Gu, M. He, K. Nagano, and H. Li, "Protecting world leaders against deep fakes," in *The IEEE Conference on Computer Vision and Pattern Recognition (CVPR) Workshops*, June 2019.

[22] Y. Li, M.-C. Chang, and S. Lyu, "In Ictu Oculi: Exposing AI Generated Fake Face Videos by Detecting Eye Blinking," *arXiv e-prints*, p. arXiv:1806.02877, Jun 2018.

[23] N. B. A. Warif, A. W. A. Wahab, M. Y. I. Idris, R. Ramli, R. Salleh, S. Shamshirband, and K.-K. R. Choo, "Copy-move forgery detection: Survey, challenges and future directions," *Journal of Network and Computer Applications*, vol. 75, pp. 259 – 278, 2016.

[24] S. Iizuka, E. Simo-Serra, and H. Ishikawa, "Globally and Locally Consistent Image Completion," *ACM Transactions on Graphics (Proc. of SIGGRAPH 2017)*, vol. 36, no. 4, pp. 107:1–107:14, 2017.

[25] A. Brock, T. Lim, J. M. Ritchie, and N. Weston, "Neural Photo Editing with Introspective Adversarial Networks," *arXiv e-prints*, p. arXiv:1609.07093, Sep 2016.

[26] D. P. Kingma, T. Salimans, R. Jozefowicz, X. Chen, I. Sutskever, and M. Welling, "Improved variational inference with inverse autoregressive flow," in *Proceedings of the 30th International Conference on Neural Information Processing Systems*, ser. NIPS'16, 2016, pp. 4743–4751.

[27] A. Tewari, M. Zollhofer, H. Kim, P. Garrido, F. Bernard, P. Perez, and C. Theobalt, "Mofa: Model-based deep convolutional face autoencoder for unsupervised monocular reconstruction," in *The IEEE International Conference on Computer Vision (ICCV)*, Oct 2017.

[28] I. Gulrajani, F. Ahmed, M. Arjovsky, V. Dumoulin, and A. C. Courville, "Improved training of wasserstein gans," in *Advances in Neural Information Processing Systems 30*, I. Guyon, U. V. Luxburg, S. Bengio, H. Wallach, R. Fergus, S. Vishwanathan, and R. Garnett, Eds., 2017, pp. 5767–5777.

[29] X. Mao, Q. Li, H. Xie, R. Y. Lau, Z. Wang, and S. Paul Smolley, "Least squares generative adversarial networks," in *The IEEE International Conference on Computer Vision (ICCV)*, Oct 2017.

[30] T. Karras, T. Aila, S. Laine, and J. Lehtinen, "Progressive growing of GANs for improved quality, stability, and variation," in *Proc. International Conference on Learning Representations (ICLR)*, 2018.

[31] P. Viola and M. J. Jones, "Robust real-time face detection," *Int. J. Comput. Vision*, vol. 57, no. 2, pp. 137–154, May 2004.

[32] W. Shen and R. Liu, "Learning residual images for face attribute manipulation," *2017 IEEE Conference on Computer Vision and Pattern Recognition (CVPR)*, pp. 1225–1233, 2017.

[33] Y. Choi, M. Choi, M. Kim, J.-W. Ha, S. Kim, and J. Choo, "Stargan: Unified generative adversarial networks for multi-domain image-to-image translation," in *The IEEE Conference on Computer Vision and Pattern Recognition (CVPR)*, June 2018.

[34] Z. He, W. Zuo, M. Kan, S. Shan, and X. Chen, "Arbitrary facial attribute editing: Only change what you want," *arXiv:1711.10678*, 2017.

[35] R. Huang, S. Zhang, T. Li, and R. He, "Beyond face rotation: Global and local perception gan for photorealistic and identity preserving frontal view synthesis," in *The IEEE International Conference on Computer Vision (ICCV)*, Oct 2017.

[36] H. Kim, P. Garrido, A. Tewari, W. Xu, J. Thies, M. Niessner, P. Pérez, C. Richardt, M. Zollhöfer, and C. Theobalt, "Deep video portraits," *ACM Trans. Graph.*, vol. 37, no. 4, pp. 163:1–163:14, Jul. 2018.

[37] J. Thies, M. Zollhöfer, M. Stamminger, C. Theobalt, and M. Nießner, "Face2Face: Real-time Face Capture and Reenactment of RGB Videos," in *Proc. Computer Vision and Pattern Recognition (CVPR), IEEE*, 2016.

[38] R. Xu, Z. Zhou, W. Zhang, and Y. Yu, "Face Transfer with Generative Adversarial Network," *arXiv e-prints*, p. arXiv:1710.06090, Oct 2017.

[39] J. Bao, D. Chen, F. Wen, H. Li, and G. Hua, "Towards open-set identity preserving face synthesis," in *The IEEE Conference on Computer Vision and Pattern Recognition (CVPR)*, June 2018.

[40] H. Ding, K. Sricharan, and R. Chellappa, "Exprgan: Facial expression editing with controllable expression intensity," *AAAI*, 2018.

[41] Z. Boulkenafet, J. Komulainen, and A. Hadid, "Face spoofing detection using colour texture analysis," *IEEE Transactions on Information Forensics and Security*, vol. 11, no. 8, pp. 1818–1830, Aug 2016.

[42] M. Barni, L. Bondi, N. Bonettini, P. Bestagini, A. Costanzo, M. Maggini, B. Tondi, and S. Tubaro, "Aligned and non-aligned double jpeg detection using convolutional neural networks," *J. Vis. Comun. Image Represent.*, vol. 49, no. C, pp. 153–163, Nov. 2017.

[43] J. Galbally and S. Marcel, "Face anti-spoofing based on general image quality assessment," in *2014 22nd International Conference on Pattern Recognition*, Aug 2014, pp. 1173–1178.

[44] V. Kushwaha, M. Singh, R. Singh, M. Vatsa, N. Ratha, and R. Chellappa, "Disguised faces in the wild," in *IEEE Conf. on Computer Vision and Pattern Recognition (CVPR) Workshops*, June 2018.

[45] S. Tariq, S. Lee, H. Kim, Y. Shin, and S. S. Woo, "Detecting both machine and human created fake face images in the wild," in *Proceedings of the 2Nd International Workshop on Multimedia Privacy and Security*, ser. MPS '18. New York, NY, USA: ACM, 2018, pp. 81–87.

[46] D. Gera and E. J. Delp, "Deepfake video detection using recurrent neural networks," in *15th IEEE International Conference on Advanced Video and Signal Based Surveillance (AVSS)*, Nov 2018, pp. 1–6.

[47] A. Khodabakhsh, R. Ramachandra, K. Raja, P. Wasnik, and C. Busch, "Fake face detection methods: Can they be generalized?" in *2018 International Conference of the Biometrics Special Interest Group (BIOSIG)*, Sep. 2018, pp. 1–6.

[48] Y. Zhang, L. Zheng, and V. L. L. Thing, "Automated face swapping and its detection," in *2017 IEEE 2nd International Conference on Signal and Image Processing (ICSIP)*, Aug 2017, pp. 15–19.

[49] P. Zhou, X. Han, V. I. Morariu, and L. S. Davis, "Two-stream neural networks for tampered face detection," in *2017 IEEE Conference on Computer Vision and Pattern Recognition Workshops (CVPRW)*, July 2017, pp. 1831–1839.

[50] H. H. Nguyen, J. Yamagishi, and I. Echizen, "Capsule-forensics: Using capsule networks to detect forged images and videos," in *ICASSP 2019 - 2019 IEEE International Conference on Acoustics, Speech and Signal Processing (ICASSP)*, 2019, pp. 2307–2311.

[51] F. Matern, C. Riess, and M. Stamminger, "Exploiting visual artifacts to expose deepfakes and face manipulations," in *IEEE Winter Applications of Computer Vision Workshops (WACVW)*, Jan 2019, pp. 83–92.

[52] P. Korshunov and S. Marcel, "Speaker inconsistency detection in tampered video," in *2018 26th European Signal Processing Conference (EUSIPCO)*, Sep. 2018, pp. 2375–2379.

[53] H. Li, B. Li, S. Tan, and J. Huang, "Detection of Deep Network Generated Images Using Disparities in Color Components," *arXiv e-prints*, p. arXiv:1808.07276, Aug 2018.

[54] A. Roy, D. Bhalang Tariang, R. Subhra Chakraborty, and R. Naskar, "Discrete cosine transform residual feature based filtering forgery and splicing detection in jpeg images," in *The IEEE Conference on Computer Vision and Pattern Recognition (CVPR) Workshops*, June 2018.

[55] Y. Li and S. Lyu, "Exposing deepfake videos by detecting face warping artifacts," in *The IEEE Conference on Computer Vision and Pattern Recognition (CVPR) Workshops*, June 2019.

[56] X. Yang, Y. Li, and S. Lyu, "Exposing deep fakes using inconsistent head poses," in *IEEE International Conference on Acoustics, Speech and Signal Processing (ICASSP)*, 2019, pp. 8261–8265.

[57] "Deepfakes," https://github.com/deepfakes/faceswap, accessed: 2020-03-16.

[58] Z. Liu, P. Luo, X. Wang, and X. Tang, "Deep learning face attributes in the wild," in *Proceedings of International Conference on Computer Vision (ICCV)*, December 2015.

[59] "Faceswap," https://github.com/MarekKowalski/FaceSwap, accessed: 2020-03-16.

[60] P. Zhou, X. Han, V. I. Morariu, and L. S. Davis, "Two-stream neural networks for tampered face detection," in *IEEE Conf. on Computer Vision and Pattern Recognition Workshops (CVPRW)*, 2017, pp. 1831–1839.

[61] N. Le and J.-M. Odobez, "Learning multimodal temporal representation for dubbing detection in broadcast media," in *Proceedings of the 24th ACM International Conference on Multimedia*, ser. MM 16. New York, NY, USA: Association for Computing Machinery, 2016, p. 202206.

[62] J. S. Chung, A. Senior, O. Vinyals, and A. Zisserman, "Lip reading sentences in the wild," in *2017 IEEE Conference on Computer Vision and Pattern Recognition (CVPR)*, 2017, pp. 3444–3453.

[63] E. Boutellaa, Z. Boulkenafet, J. Komulainen, and A. Hadid, "Audiovisual synchrony assessment for replay attack detection in talking face biometrics," *Multimedia Tools Appl.*, vol. 75, no. 9, pp. 5329 – 5343, May 2016.

[64] P. Korshunov and S. Marcel, "Deepfakes: a new threat to face recognition? assessment and detection," *CoRR*, vol. abs/1812.08685, 2018.

[65] H.-Y. Wu, M. Rubinstein, E. Shih, J. Guttag, F. Durand, and W. Freeman, "Eulerian video magnification for revealing subtle changes in the world," *ACM Trans. Graph.*, vol. 31, no. 4, pp. 65:1–65:8, Jul. 2012.

[66] W. Chen and D. McDuff, "Deepphys: Video-based physiological measurement using convolutional attention networks," in *The European Conference on Computer Vision (ECCV)*, September 2018.

[67] P. V. Rouast, M. T. P. Adam, R. Chiong, D. Cornforth, and E. Lux, "Remote heart rate measurement using low-cost rgb face video: a

technical literature review," *Frontiers of Computer Science*, vol. 12, no. 5, pp. 858–872, Oct 2018.
[68] M.-Z. Poh, D. J. McDuff, and R. W. Picard, "Non-contact, automated cardiac pulse measurements using video imaging and blind source separation." *Opt. Express*, vol. 18, no. 10, pp. 10 762–10 774, May 2010.
[69] G. Balakrishnan, F. Durand, and J. Guttag, "Detecting pulse from head motions in video," in *2013 IEEE Conference on Computer Vision and Pattern Recognition*, June 2013, pp. 3430–3437.
[70] G. de Haan and V. Jeanne, "Robust pulse rate from chrominance-based rppg," *IEEE Transactions on Biomedical Engineering*, vol. 60, no. 10, pp. 2878–2886, Oct 2013.
[71] C. Zhao, C.-L. Lin, W. Chen, and Z. Li, "A novel framework for remote photoplethysmography pulse extraction on compressed videos," in *The IEEE Conference on Computer Vision and Pattern Recognition (CVPR) Workshops*, June 2018.
[72] L. Feng, L. Po, X. Xu, Y. Li, and R. Ma, "Motion-resistant remote imaging photoplethysmography based on the optical properties of skin," *IEEE Transactions on Circuits and Systems for Video Technology*, vol. 25, no. 5, pp. 879–891, May 2015.
[73] S. K. A. Prakash and C. S. Tucker, "Bounded kalman filter method for motion-robust, non-contact heart rate estimation," *Biomed. Opt. Express*, vol. 9, no. 2, pp. 873–897, Feb 2018.
[74] S. Tulyakov, X. Alameda-Pineda, E. Ricci, L. Yin, J. F. Cohn, and N. Sebe, "Self-adaptive matrix completion for heart rate estimation from face videos under realistic conditions," in *The IEEE Conference on Computer Vision and Pattern Recognition (CVPR)*, June 2016.
[75] "Fakeapp," https://www.malavida.com/en/soft/fakeapp/, accessed: 2020-03-16.
[76] "Faceswap-gan," https://github.com/shaoanlu/faceswap-GAN, accessed: 2020-03-16.
[77] J. Thies, M. Zollhöfer, and M. Nießner, "Deferred neural rendering: Image synthesis using neural textures," *ACM Trans. Graph.*, vol. 38, no. 4, Jul. 2019. [Online]. Available: https://doi.org/10.1145/3306346.3323035
[78] N. Dufour, A. Gully, P. Karlsson, A. V. Vorbyov, T. Leung, J. Childs, and C. Bregler, "Deepfakes detection dataset by google & jigsaw."
[79] S. Butterworth *et al.*, "On the theory of filter amplifiers," *Wireless Engineer*, vol. 7, no. 6, pp. 536–541, 1930.
[80] A. S. M. Murugavel, S. Ramakrishnan, K. Balasamy, and T. Gopalakrishnan, "Lyapunov features based eeg signal classification by multiclass svm," in *2011 World Congress on Information and Communication Technologies*, Dec 2011, pp. 197–201.
[81] S. Pei and J. Ding, "Relations between gabor transforms and fractional fourier transforms and their applications for signal processing," *IEEE Transactions on Signal Processing*, vol. 55, no. 10, pp. 4839–4850, Oct 2007.
[82] M. Soleymani, J. Lichtenauer, T. Pun, and M. Pantic, "A multimodal database for affect recognition and implicit tagging," *IEEE Trans. Affect. Comput.*, vol. 3, no. 1, pp. 42–55, Jan. 2012.
[83] H. Hu, Y. Wang, and J. Song, "Signal classification based on spectral correlation analysis and svm in cognitive radio," in *22nd International Conference on Advanced Information Networking and Applications (aina 2008)*, March 2008, pp. 883–887.
[84] A. Kampouraki, G. Manis, and C. Nikou, "Heartbeat time series classification with support vector machines," *IEEE Trans. on Information Technology in Biomedicine*, vol. 13, no. 4, pp. 512–518, July 2009.
[85] N. Jatupaiboon, S. Pan-Ngum, and P. Israsena, "Real-time eeg-based happiness detection system," in *TheScientificWorldJournal*, 2013.
[86] W. Zhang, "Automatic modulation classification based on statistical features and support vector machine," in *2014 XXXIth URSI General Assembly and Scientific Symposium (URSI GASS)*, Aug 2014, pp. 1–4.
[87] D. Nie, X. Wang, L. Shi, and B. Lu, "Eeg-based emotion recognition during watching movies," in *2011 5th International IEEE/EMBS Conference on Neural Engineering*, April 2011, pp. 667–670.
[88] G. Koren, "Wearable sensor for physiological data acquisition in early education," https://github.com/get/PPG-Heart-Rate-Classifier/blob/master/thesis%20excerpt.pdf, 2016, accessed: 2018-11-15.
[89] C. Cortes and V. Vapnik, "Support-vector networks," *Machine Learning*, vol. 20, no. 3, pp. 273–297, Sep 1995.
[90] S. Fortune, "Handbook of discrete and computational geometry." Boca Raton, FL, USA: CRC Press, Inc., 1997, ch. Voronoi Diagrams and Delaunay Triangulations, pp. 377–388.
[91] MATLAB, *version R2018a*. Natick, Massachusetts: The MathWorks Inc., 2010.
[92] B. Amos, B. Ludwiczuk, and M. Satyanarayanan, "Openface: A general-purpose face recognition library with mobile applications," CMU-CS-16-118, CMU School of Computer Science, Tech. Rep., 2016.
[93] C.-C. Chang and C.-J. Lin, "Libsvm: A library for support vector machines," *ACM Trans. Intell. Syst. Technol.*, vol. 2, no. 3, pp. 27:1–27:27, May 2011.
[94] J. Buckheit, J. B. Buckheit, D. L. Donoho, and D. L. Donoho, "Wavelab and reproducible research." Springer-Verlag, 1995, pp. 55–81.
[95] F. Chollet *et al.*, "Keras," https://github.com/fchollet/keras, 2015.
[96] C. Szegedy, V. Vanhoucke, S. Ioffe, J. Shlens, and Z. Wojna, "Rethinking the inception architecture for computer vision," in *IEEE Conf. on Computer Vision and Pattern Recognition (CVPR)*, June 2016.
[97] F. Chollet, "Xception: Deep learning with depthwise separable convolutions," in *The IEEE Conference on Computer Vision and Pattern Recognition (CVPR)*, July 2017.
[98] X. SHI, Z. Chen, H. Wang, D.-Y. Yeung, W.-k. Wong, and W.-c. WOO, "Convolutional lstm network: A machine learning approach for precipitation nowcasting," in *Advances in Neural Information Processing Systems 28*, 2015, pp. 802–810.
[99] L. Silva, O. P. Bellon, and K. L. Boyer, "Precision range image registration using a robust surface interpenetration measure and enhanced genetic algorithms," *IEEE Transactions on Pattern Analysis & Machine Intelligence*, vol. 23, no. 05, pp. 762–776, may 2005.
[100] S. Mika, G. Ratsch, J. Weston, B. Scholkopf, and K. R. Mullers, "Fisher discriminant analysis with kernels," in *Neural Networks for Signal Processing IX: Proceedings of the 1999 IEEE Signal Processing Society Workshop (Cat. No.98TH8468)*, Aug 1999, pp. 41–48.
[101] S. Wold, K. Esbensen, and P. Geladi, "Principal component analysis," *Chemometrics and Intelligent Laboratory Systems*, vol. 2, no. 1, pp. 37 – 52, 1987, proceedings of the Multivariate Statistical Workshop for Geologists and Geochemists.
[102] Z. J. Koles, M. S. Lazar, and S. Z. Zhou, "Spatial patterns underlying population differences in the background eeg," *Brain Topography*, vol. 2, no. 4, pp. 275–284, Jun 1990.
[103] P. Welch, "The use of fast fourier transform for the estimation of power spectra: A method based on time averaging over short, modified periodograms," *IEEE Transactions on Audio and Electroacoustics*, vol. 15, no. 2, pp. 70–73, June 1967.

Umur Aybars Ciftci received his MSc degree in computer science from Binghamton University in 2014. He is currently a PhD candidate in the computer science department of Binghamton University where he is a member of Graphics and Image Computing Laboratory. His research interests are in computer vision, human computer interaction, and affective computing.

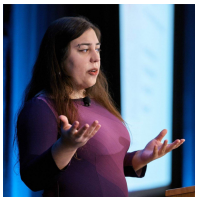

Ilke Demir earned her PhD degree in Computer Science from Purdue University, focusing on 3D vision approaches for generative models, urban reconstruction and modeling, and computational geometry for synthesis and fabrication. Afterwards, Dr. Demir joined Facebook as a Postdoctoral Research Scientist working with Ramesh Raskar from MIT. Her research included human behavior analysis via deep learning in virtual reality, geospatial machine learning, and 3D reconstruction at scale. In addition to her publications in top-tier venues (SIGGRAPH, ICCV, CVPR), she has organized workshops, competitions, and courses in the intersection of deep learning and computer vision. She has received several awards and honors such as Jack Dangermond Award, Bilsland Dissertation Fellowship, and Industry Distinguished Lecturer, in addition to her best paper/poster/reviewer awards. Currently she leads the research efforts on 3D vision and deep learning approaches in the world's largest volumetric capture stage at Intel Studios.

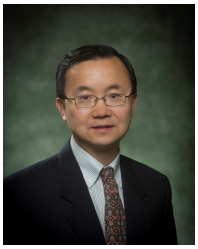

Lijun Yin Lijun Yin is a Professor of Computer Science, Director of Center for Imaging, Acoustics, and Perception Science at Binghamton University, Director of Graphics and Image Computing Laboratory, and Co-director of Seymour Kunis Media Core, T. J Watson School of Engineering and Applied Science at the State University of New York at Binghamton. He received Ph.D. of computer science from the University of Alberta and Master of Electrical Engineering from Shanghai Jiao Tong University. Dr. Yin's research focuses on computer vision, graphics, HCI, and multimedia, specifically on face and gesture modeling, analysis, recognition, animation, and expression understanding. His research has been funded by the NSF, AFRL/AFOSR, NYSTAR, and SUNY Health Network of Excellence. Dr. Yin received the prestigious Lois B. DeFleur Faculty Prize for Academic Achievement Award (2019), James Watson Investigator Award of NYSTAR (2006), and SUNY Chancellor's Award for Excellence in Scholarship & Creative Activities (2014). He holds 11 US patents, and released four 2D/3D/4D facial expression databases to public, and has published over 150 papers in technical conferences and journals. Dr. Yin served as a program co-chair of FG 2013 and FG2018. He is currently serving on editorial board of IVC and PRL.